MODELING AND SIMULATION OF MICROPOLAR FLOW AND THERMAL RADIATION IN POROUS MEDIA

by

Ibrahim MAHARIQ[a,b,c,d], Kashif ULLAH[e], Mehreen FIZA[e], Hakeem ULLAH[e*], Ali AKGUL[f,g,h,i], Ghada R. ELNAGGAR[j], Ilyas KHAN[k], and Wei Sin KOH[l]

[a] College of Engineering and Architecture, Gulf University for Science and Technology, Mishref, Kuwait
[b] University College, Korea University, Seoul, South Korea
[c] Department of Medical Research, China Medical University Hospital, China Medical University, Taichung, Taiwan
[d] Applied Science Research Center, Applied Science Private University, Amman, Jordan
[e] Department of Mathematics, Abdul Wali Khan University, Mardan, Khyber Pakhtunkhwa, Pakistan
[f] Department of Electronics and Communication Engineering, Saveetha School of Engineering, SIMATS, Chennai, Tamilnadu, India
[g] Siirt University, Art and Science Faculty, Department of Mathematics, Siirt, Turkey
[h] Applied Science Research Center, Applied Science Private University, Amman, Jordan
[i] Department of Computer Engineering, Biruni University, Topkapı, Istanbul, Turkey
[j] Department of Industrial and Systems Engineering, College of Engineering, Princess Nourah bint Abdulrahman University, Riyadh, Saudi Arabia
[k] Department of Mathematics, College of Science Al-Zulfi, Majmaah University, Al-Majmaah, Saudi Arabia
[l] INTI International University, Persiaran Perdana BBN Putra Nilai, Nilai, Negeri Sembilan, Malaysia

Original scientific paper
https://doi.org/10.2298/TSCI2504075M

Recurrent neural networks (RNN) have attracted attention in the academic community because of their capability to handle intricate, non-linear models. The RNN, with their strong pattern recognition abilities, are therefore well-equipped to be applied in intricate fields such as fluid dynamics, biological computing, and biotechnology. This study investigates the effectiveness of the Levenberg-Marquardt algorithm combined with recurrent neural networks (LMA-RNN) is simulating the heat transfer of a micropolar fluid through a porous medium with radiation (HTMFPMR) model. In this research, data is obtained using the Adams numerical technique and later optimized through the application of LMA-RNN. The LMA-RNN approach divides the data by using 80% for training, 10% for testing, and the remaining 10% for validation purposes. The velocity and temperature distributions are presented, and the effects of the inertia coefficient, microrotation, radiation parameter, and Prandtl number on the heat transfer are thoroughly analyzed. An upsurge in the permeability constraint outcomes in a rise in angular velocity and temperature, while causing a reduction in velocity. As the vortex-viscosity constraint increases, both the velocity and angular velocity show an upward trend. The temperature field declines with rise radiation constraint. Mean squared error (MSE), regression plots, and error histograms are used to

* Corresponding authors, e-mail: hakeemullah1@gmail.com; aliakgul00727@gmail.com

assess the performance of the LMA-RNN that have been applied. Reduced MSE indicates more accurate model predictions, validating the proposed strategy.

Key words: *micropolar fluid, RNN, heat transfer and thermal radiation, smart grid, porous medium*

Introduction

The phenomenon of heat transfer happens naturally when there is a temperature differential and heat move from one object to another or within the same object. Fourier was the first to propose the now-famous *Fourier's law of heat conduction* in this direction. Nevertheless, this law falls short of fully capturing the features of the heat transfer phenomenon. For many applications, including evaporators, condensers, air conditioning systems, and power plants, a high rate of heat transfer is the primary objective. As a result, several strategies to rise the rate of heat transfer were put forth by scientists and engineers. Duwairi *et al.* [1] investigated the heat transfer characteristics of a viscous fluid being squeezed and extruded between two parallel plates, as reported in *Heat and Mass Transmission.* Mahmood *et al.* [2] studied squeezed flow with heat transfer over a porous plate. Mustafa [3] explored the heat transfer properties of an upper-convected spinning Maxwell fluid flow using the Cattaneo-Christov heat flux model (CCHFM). Han *et al.* [4] presented heat transfer in a viscoelastic fluid using the CCHFM. Heat transfer increases in natural convection nanofluid flow over a vertical plate with energy and viscous dissipation were deliberate by Sheri and Thumma [5]. The effects of MHD slip flow and heat transfer of nanofluid on an extending cylinder were observed by Poply *et al.* [6]. Sheikholeslami *et al.*'s [7] study used nanofluid to investigate MHD natural convection heat transfer. The influence of fundamental parameters on the thermal and velocity field of Cu-water and Al_2O_3 nanoparticles was explored by Thumma *et al.* [8]. Gireesha *et al.* [9] analyzed MHD flow, along with heat and mass transfer, in a radiative Eyring-Powell nanofluid over a 3-D stretching surface.

The theory of micropolar fluids has attracted considerable attention in recent years, as conventional Newtonian fluids cannot properly represent the characteristics of fluids containing suspended particles. Physically, non-Newtonian fluids such as animal blood, polymer fluids, fluid suspensions, and dumbbell-shaped or short rigid cylindrical elements can all be found in micropolar fluids. Micropolar fluid dynamics can also be used to model the presence of specific particles, such as smoke or dust, in a gas. Eringen [10] was the first to develop the theory of micropolar fluids. In addition to the standard equations for Newtonian fluid flow, his theory presents new constitutive equations, new material constraints, and the microrotation, an additional independent vector field. There is a wealth of literature in the field of micropolar fluids, covering many facets of the issue. Among them are Gorla [11], researchers Rees and Bassom [12] looked into how a micropolar fluid flowed over a flat plate and well as Desseaux and Kelson [13], who investigated the movement of micropolar fluids on surfaces that stretch. The numerical methods [14-17] are used for the solutions of various nonlinear problems in engineering. The numerical methods have some merits and dermirites like discretization, linearization and sensitive to initial guess assumptions [18-21]. In addition to numerical methods analytical methods are also used for the nonlinear problems [22-25], The analytical methods also have some limitiions like assumption of small paralater, required initial guees [26-28]. To avoid these issues artificial intelligence (AI) has recently been useful to solve numerous linear and non-linear problems, including the use of an integrated computational intelligence approach for non-linear boundary value problems [29-32].

This study aims to investigate HTMFPMR model using LMA-RNN.

Governing equation

Consider about the incompressible micropolar fluids in two dimensions. The semi-infinite horizontal plate with the region $y > 0$ is being traversed by the micropolar fluid via a porous media. The heat transfer phenomenon and the thermal radiation effect are taken into explanation for the permeable medium and the micopolar fluid. Figure 1(a) provides the geometry of the flow problem. The basic formulas are provided as [33]:

$$u_x + v_y = 0 \tag{1}$$

$$uu_x + vu_y = \nu u_{yy} + k_1 \varpi_y + \frac{\nu\phi}{k}U - \frac{\nu\phi}{k}u + C\phi U^2 - C\phi u^2 \tag{2}$$

$$g_1 \varpi_{yy} = 2\varpi + \varpi_y \tag{3}$$

$$uT_x + vT_y = \frac{1}{\rho c_p}(kT_{yy} - q_y) \tag{4}$$

Incorporating boundary conditions [20]:

$$\begin{gathered} u = 0, \quad v = 0, \quad \varpi = 0, \quad T = T_w, \quad \text{at} \quad y = 0, \\ u = U_0, \quad \varpi = 0, \quad T = T_\infty, \quad \text{at} \quad y \to \infty \end{gathered} \tag{5}$$

where $k_1 = \rho s, \nu = \dfrac{(\mu + s)}{\rho}$.

We introduce the following transformations.

$$\varphi(x, y) = \sqrt{2\nu U_0 x}\, f(\eta), \quad \varpi = \sqrt{\frac{U_0}{2\nu x}} U_0 g(\eta), \quad \eta = \sqrt{\frac{U_0}{2\nu x}} y, \quad \theta = \frac{T - T_\infty}{T_w - T_\infty} \tag{6}$$

where φ is the stream function and defined as $u = \varphi_y$ and $v = -\varphi_x$. By applying eq. (9), the governing equations simplify to the following form:

$$f''' + ff'' + Ag' + \frac{1}{M}(1 - f') + N(1 - f'^2) = 0 \tag{7}$$

$$Sg'' - 2(2g + f'') = 0 \tag{8}$$

$$(3R + 4)\theta'' + 3R\Pr f\theta' = 0 \tag{9}$$

With boundary conditions:

$$\begin{gathered} f = 0, \quad f' = 0, \quad g = 0, \quad \theta = 1, \quad \text{at} \quad \eta = 0 \\ f' \to 1, \quad g \to 0, \quad \theta \to 0, \quad \text{at} \quad \eta \to \infty \end{gathered} \tag{10}$$

where

$$A=\frac{k_1}{\nu},\quad M=\frac{kU_0}{2\phi\nu x},\quad N=2\phi c_x,\quad S=\frac{g_1U_0}{\nu x},\quad R=\frac{k^*k}{4\varpi^*T^3}\quad \text{and}\quad \Pr=\frac{\rho\nu c_p}{k}$$

are the coupling constant, permeability, inertia coefficient, microrotation, radiation parameter, and Prandtl number.

Numerical method

Results analysis and discussion

Performance and error plots

The outcom of LMA-RNN for case one of all six senarios in relations of performance function and states are showing in fig. 1(c), and 1(f). The error histograms and series time response are assumed in fig. 1(e) and 1(f). Regression of the results for six for the cases one is demonstrated in fig. 1(g), for the six senarios of flow HTMFPMR. For individually situation of the flow HTMFPMR model, all three cases were evaluated in terms of epochs used, performance function, backpropagation plans, and execution time. In fig. 1(c) convergence of MSE for time reversal procedure are present for case one of all scenarios of flow problem. One may see that the best network performance function attain $2.5915\cdot10^{-10}$ at epochs 1000. The approximate values of the slope and learning rate (Mu) in backpropagation are [0.00-2426] and [E-7] as exposed in fig. 1(d). The results demonstrate the accurate and convergent performance function of LMA-RNN in each case. Figures 1(e) and 1(h) show the error visualisations and time seriese responese are shown in fig. 1(f). Figure 1(e) shows the error histogram plot, while fig. 1(f) shows the error analysis plots. The uppermost error attain for time reversal are fewer than $56\cdot10^{-5}$ for case one of all 1 to 6 scenarios. The error subtleties are more calculated with error histogram for each contribution point and consequences are given in fig. 1(e), for case one of all 1 to 6 scenarios, respectively, of flow HTMFPMR model. The error silo with situation zero line has error around $-7.1\cdot10^{-8}$ for all 1 to 6 scenarios of flow HTMFPMR model. Figure 1(h) show error auto-correlations. Figure 1(h) show the auto-correlation error one. The error is $10\cdot10^{-11}$. Figure 1(g) show the regression plots.

Velocity and temperature profiles

This section presents a graph-based discussion of the behaviour of several physical parameters that surfaced during the numerical simulation of the problem on the velocity and temperature field. Findings are obtained for a range of radiation constraints, R, coupling constant, A, inertia coefficient, N, permeability parameter, M, microrotation constraint, S, and Prandtl number. The effects of these parameters were investigated along fig. 2 for fluid velocity, thermal and angular velocity field of micro-structures. Figure 2(i) illustrates how fluid velocity profile $f'(\eta)$ drops as permeability constraint M increases. Increasing permeability corresponds to a decrease in porosity, which in turn reasons a reduction in $f'(\eta)$. The velocity profile of micro-structures, $g(\eta)$, decreased as M increased, as shown in fig. 2(ii). This increased resistance impedes the motion of the fluid, resulting in a reduction in the velocity of micro-structures within the fluid. The dimensionless temperature profile, $\theta(\eta)$, rises as M increases, as shown in fig. 2(iii). This aligns with what we expect as the velocity declines. Figures 2(iv)-2(vi) present the properties of varying the vortex-viscosity constraint, A, on the temperature, fluid speed, and angular velocity of the micro-structures. It is experiential that as coupling constraint A upsurge, the fluid field and the angular velocity of the micro-structure $g(\eta)$ upsurge. As coupling constraint, A rise from $0 \leq 0.2$ the velocity filed decrease and then increase from $0.2 \leq 1$, results shown in the fig 2(iv). Figure 2(v) illustrates the effect of coupling constraint A on g. When A increases within the range $0 \leq 0.2$ velocity decreases. However, as A

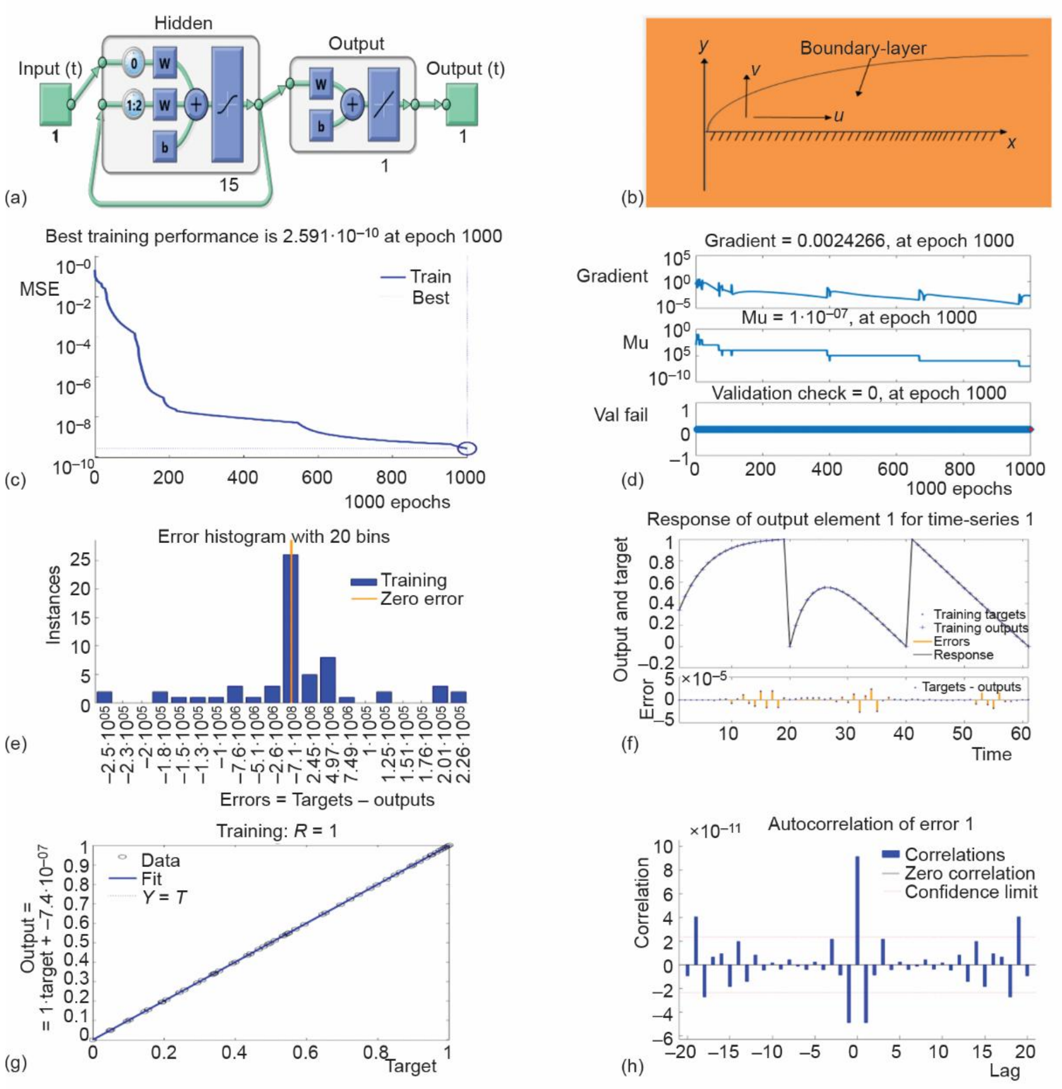

Figure 1. The output of projected LMA-RNN for HTMFPMR

continues to increase in the range $0.2 \leq 1$, the velocity increases. Figure 2(vi) demonstrates the outcome of parameter A on the temperature distribution, θ. As the volume of A increases, the temperature distribution profile increases. The output inertia coefficient parameter N, is displayed in fig. 2(vii), which shows the outcome of the inertia coefficient parameter in f'. As the value of N upsurges, the velocity profile declines. Figure 2(viii) show the effect of inertia coefficient constraint in velocity profile of micro-structures $g(\eta)$. As the value of N increases, the velocity field increases. Figure 2(ix) shows the result of microrotation constraint S. As the value of S rises, the velocity profile also increases. The influence of radiation on the dimensionless thermal distribution θ is shown in fig. 2(x). We observed that the thermal profile declines.

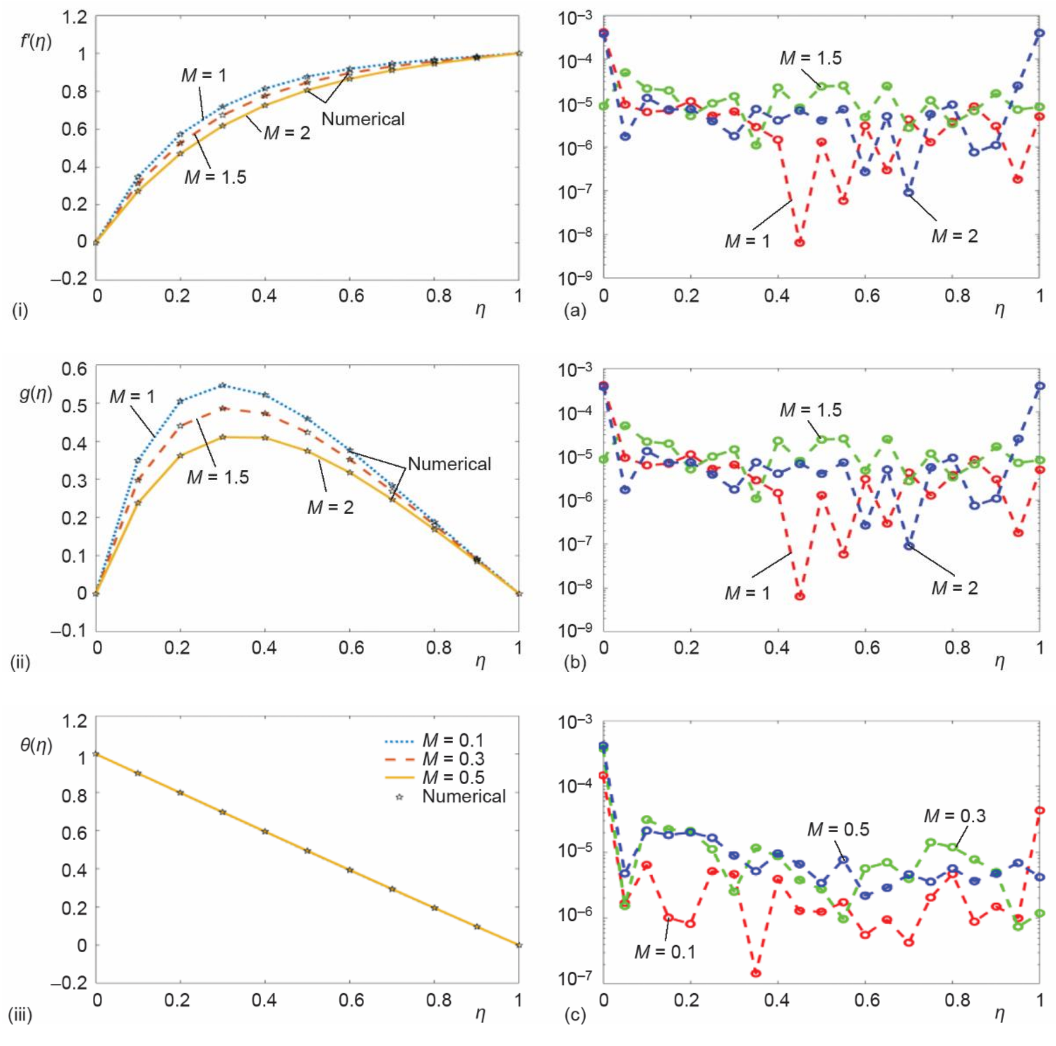

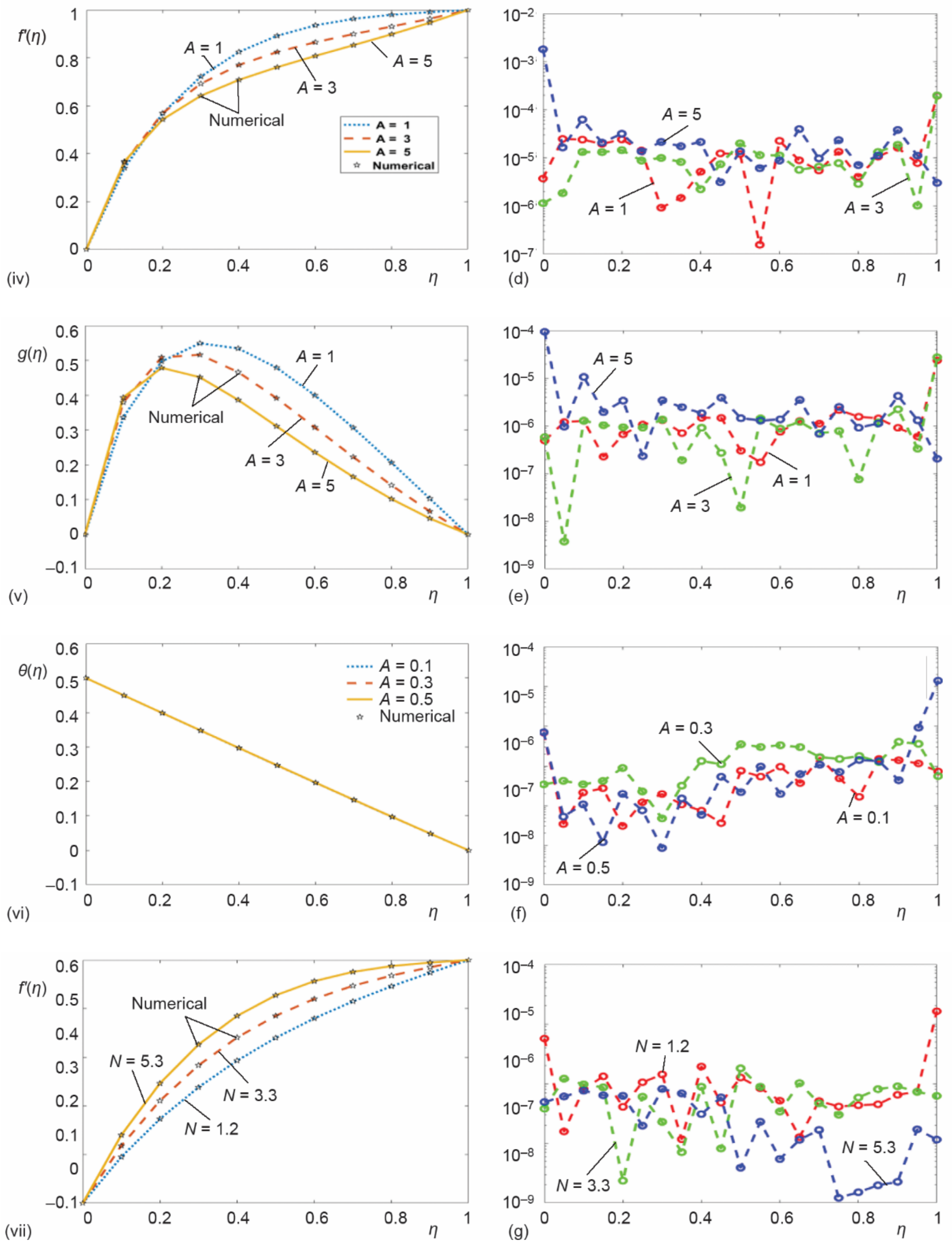
f′(η)
A = 1
A = 3
A = 5
Numerical
(iv)
η
A = 5
A = 1
A = 3
(d)
η
g(η)
A = 1
Numerical
A = 3
A = 5
(v)
η
A = 5
A = 1
A = 3
(e)
η
θ(η)
A = 0.1
A = 0.3
A = 0.5
Numerical
(vi)
η
A = 0.3
A = 0.1
A = 0.5
(f)
η
f′(η)
Numerical
N = 5.3
N = 3.3
N = 1.2
(vii)
η
N = 1.2
N = 5.3
N = 3.3
(g)
η

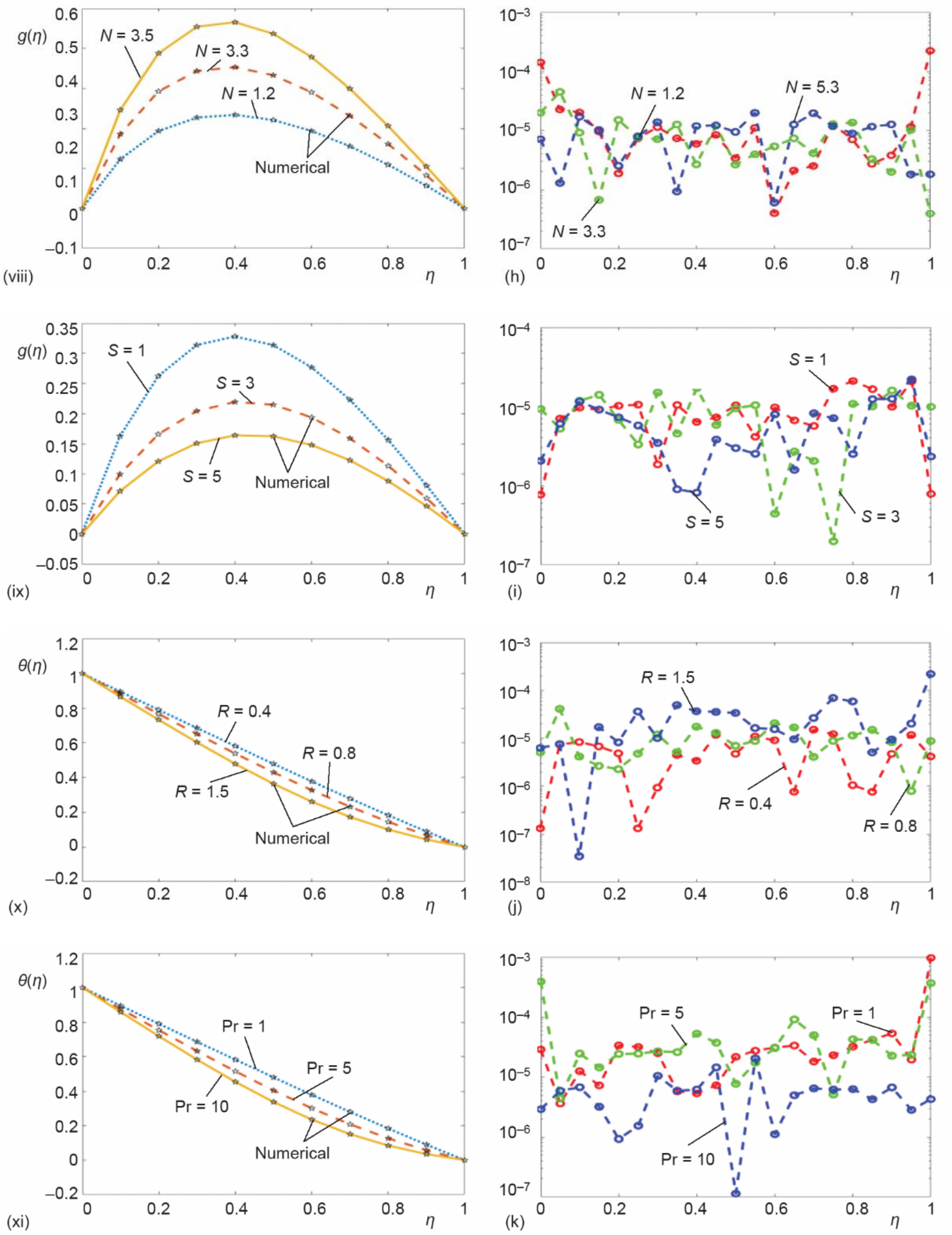

Figure 2. Evaluation of the proposed LMA-RNN for HTMFPMR

Figure 2(xi) illustrates the outcome of the Prandtl number in θ. The value of Prandtl number increases the thermal distribution decreases. The outcome *AE*, from suggestion solutions is determine and results are displayed in subfigures 2(a)-2(k) for case trainings 1-6, it the absolute error is around 10^{-8} to 10^{-3}, 10^{-6} to 10^{-4}, 10^{-7} to 10^{-3}, 10^{-8} to 10^{-3}, 10^{-6} to 10^{-4}, 10^{-6} to 10^{-3}, 10^{-7} to 10^{-4}, 10^{-6} to 10^{-3}, 10^{-6} to 10^{-3}, 10^{-7} to 10^{-4}, 10^{-6} to 10^{-4}, 10^{-5} to 10^{-3}, 10^{-7} to 10^{-5}, 10^{-8} to 10^{-4}, 10^{-7} to 10^{-4}, 10^{-7} to 10^{-5}, 10^{-6} to 10^{-4}, 10^{-7} to 10^{-3}, 10^{-6} to 10^{-4}, 10^{-7} to 10^{-5}, 10^{-7} to 10^{-5}, 10^{-6} to 10^{-4}, 10^{-6} to 10^{-4}, 10^{-6} to 10^{-5}, 10^{-6} to 10^{-5}, 10^{-7} to 10^{-5}, 10^{-6} to 10^{-5}, 10^{-7} to 10^{-5}, 10^{-8} to 10^{-4}, 10^{-8} to 10^{-4}, 10^{-6} to 10^{-3}, 10^{-6} to 10^{-3}, and 10^{-7} to 10^{-5}, for all scenarios, respectively.

Tables interpretation

The result of technique of LMA-RNN for resolve each one case of all 1-6 scenarios of flow for HTMFPMR model are present in tab. 1. The performance function of LMA-RNN is about 10^{-21} to 10^{-10}, 10^{-22} to 10^{-12}, 10^{-25} to 10^{-11}, 10^{-19} to 10^{-11}, and 10^{-10} to 10^{-23} for individual six scenarios cases of flow HTMFPMR model. These consequences demonstrate the consistent performance function of LMA-RNN for solving flow HTMFPMR model.

Table 1. Consequence of LMA-RNN for Scenario six of HTMFPMR

Case	MSE	Performance	Gradient	*Mu*	Epoch	Time
	Training					
1	$2.59\cdot10^{-10}$	$2.591\cdot10^{-10}$	0.0024226	$1.00\cdot10^{-7}$	1000	34
2	$2.18\cdot10^{-21}$	$2.18\cdot10^{-21}$	$2.456\cdot10^{-6}$	$1.00\cdot10^{-7}$	750	30
3	$5.95\cdot10^{-11}$	$5.95\cdot10^{-11}$	$1.54\cdot10^{-7}$	$1.00\cdot10^{-7}$	1000	36
1	$1.5364\cdot10^{-12}$	$1.5364\cdot10^{-12}$	$9.917\cdot10^{-8}$	$1.00\cdot10^{-8}$	718	19
2	$2.492\cdot10^{-10}$	$2.492\cdot10^{-10}$	0.000420	$1.00\cdot10^{-6}$	1000	36
3	$1.10\cdot10^{-13}$	$1.10\cdot10^{-13}$	$9.98\cdot10^{-8}$	$1.00\cdot10^{-8}$	802	29
1	$1.2746\cdot10^{-19}$	$1.2746\cdot10^{-19}$	$1.491\cdot10^{-8}$	$1.00\cdot10^{-8}$	176	35
2	$1.02\cdot10^{-22}$	$1.02\cdot10^{-22}$	$1.65\cdot10^{-11}$	$1.00\cdot10^{-8}$	190	25
3	$2.03\cdot10^{-12}$	$2.03\cdot10^{-12}$	$1.05\cdot10^{-6}$	$1.00\cdot10^{-8}$	1000	37
1	$4.9241\cdot10^{-11}$	$4.9241\cdot10^{-11}$	$1.0819\cdot10^{-6}$	$1.00\cdot10^{-7}$	1000	30
2	$7.66\cdot10^{-21}$	$7.66\cdot10^{-21}$	$1.45\cdot10^{-8}$	$1.00\cdot10^{-11}$	416	14
3	$1.55\cdot10^{-25}$	$1.55\cdot10^{-25}$	$2.40\cdot10^{-12}$	$1.00\cdot10^{-10}$	130	23
1	$9.1242\cdot10^{-11}$	$9.1242\cdot10^{-11}$	$1.0634\cdot10^{-8}$	$1.00\cdot10^{-11}$	30	6
2	$1.45\cdot10^{-19}$	$1.45\cdot10^{-19}$	$8.26\cdot10^{-9}$	$1.00\cdot10^{-10}$	14	3
3	$8.12\cdot10^{-13}$	$8.12\cdot10^{-13}$	$1.34\cdot10^{-7}$	$1.00\cdot10^{-8}$	1000	36
1	$5.2144\cdot10^{-12}$	$5.2144\cdot10^{-12}$	$9.97738\cdot10^{-8}$	$1.00\cdot10^{-8}$	739	35
2	$1.29\cdot10^{-10}$	$1.29\cdot10^{-10}$	$3.367\cdot10^{-6}$	$1.00\cdot10^{-7}$	1000	37
3	$1.33\cdot10^{-23}$	$1.33\cdot10^{-23}$	$1.448\cdot10^{-11}$	$1.00\cdot10^{-9}$	16	10

Concluding remarks

In this study, the influence of radiation on the heat transfer behavior of a micropolar fluid over a fixed horizontal plate within a porous medium. Using similarity variables, the system of PDE is simplified into a system of ODE. The *A* recently presented intelligent computing approache, known as LMA-RNN, is utilized to analyze the HTMFPMR model. The accuracy and stability of the LMA-RNN approach vary from 10^{-12} to 10^{-3}, as seen in the comparison between the proposed model and conventional outcome.

- A rise in the permeability constraint leads to higher angular velocity and thermal but a reduction in flow velocity.
- An upsurge in the inertia coefficient parameter, *N*, leads to reduction in the fluid velocity profile, but the micro-structure velocity profile increases.
- Compared to Newtonian fluids, micropolar fluids demonstrate drag-reduction behavior.
- As the vortex-viscosity constraint raises, there is a corresponding upsurge in velocity and angular velocity.
- The temperature profile declines with an upsurge in the radiation parameter and Prandtl number.
- To compute the friction factor and heat transfer rate, wall values of velocity, angular velocity, and temperature are tabulated and analyzed.

Nomenclature

A – coupling strength
C – non-Darcy flow coefficient
c_p – specific temperture
f – non-dimensional velocity expression
g – non-dimensional microrotation angular velocity expression
k – porous medium permeability
k_1 – coupling constant
M – permeability constraint
N – inertia coefficient parameter
Pr – Prandtl number
R – radiation constraint
S – microrotation constraint
s – constant characteristic to the fluid
T – temperature field
u – velocity along *x*-axis
U_0 – steady stream velocity
v – velocity along *y*-axis
w – surface conditions
x – surface distance
y – distance normal to the surface
∞ – free-stream conditions

Greek symbols

ϕ – permeability
ν – kinematic viscosity
θ – dimensionless temperature
μ – dynamical viscosity
ρ – density of fluid
σ – angular velocity

Acknowledgment

The authors extend their appreciation to the support of funding received from Princess Nourah bint Abdulrahman University Researchers Supporting Project number (PNURSP2025R914), Princess Nourah bint Abdulrahman University, Riyadh, Saudi Arabia.

References

[1] Duwairi, H. M., *et al.*, On Heat Transfer Effects of a Viscous Fluid Squeezed and Extruded Between Two Parallel Plates, *Heat Mass Transf., 14* (2004), Aug., pp. 112-117
[2] Mahmood, M., *et al.*, Squeezed Flow and Heat Transfer over a Porous Surface for Viscous Fluid, *Heat Mass Transf., 44* (2007), Feb., pp. 165-173
[3] Mustafa, M., Cattaneo-Christov Heat Flux Model for Rotating Flow and Heat Transfer of Upper-Convected Maxwell Fluid, *AIP Adv., 5* (2015), 047109

[4] Han, S., *et al.*, Coupled Flow and Heat Transfer in Viscoelastic Fluid with Cattaneo-Christov Heat Flux Model, *Appl. Math. Lett., 38* (2014), Dec., pp. 87-93
[5] Sheri, S. R., Thumma, T., Numerical Study of Heat Transfer Enhancement in MHD Free Convection Flow over Vertical Plate Utilizing Nanofluids, *Ain Shams Eng. J., 9* (2018), 4, pp. 1169-1180
[6] Poply, V., *et al.*, Stability Analysis of MHD Outer Velocity Flow on a Stretching Cylinder, *Alexandria Eng. J., 57* (2017), 3, pp. 2077-2083
[7] Sheikholeslami, M., *et al.*, Lattice Boltzmann Method for MHD Natural Convection Heat Transfer Using Nanofluid, *Powder Technol., 254* (2014), Mar., pp. 82-93
[8] Thumma, T., *et al.*, Numerical Study of Heat Source/Sink Effects on Dissipative Magnetic Nanofluid Flow from a Non-Linear Inclined Stretching/Shrinking Sheet, *J. Mol. Liq., 232* (2017), Apr., pp. 159-173
[9] Gireesha, B., *et al.*, Effect of Suspended Nanoparticles on Three-Dimensional MHD Flow, Heat and Mass Transfer of Radiating Eyring-Powell Fluid over a Stretching Sheet, *Journal of Nanofluids, 4* (2015), 4, pp. 474-484
[10] Eringen, A. C., Theory of Micropolar Fluids, *J. Math. Mech., 16* (1966), 1, pp. 1-18
[11] Gorla, R. S., Heat Transfer in Micropolar Boundary Layer Flow over a Flat Plate, *Int. J. Eng. Sci., 21* (1983), 7, pp. 791-796
[12] Rees, D. A. S., Bassom, A.P., The Blasius Boundary-Layer Flow of a Micropolar Fluid, *Int. J. Eng. Sci., 34* (1996), 1, pp. 113-124
[13] Kelson, N. A., Desseaux, A., Effect of Surface Conditions on Flow of a Micropolar Fluid Driven by a Porous Stretching Sheet, *Int. J. Eng. Sci., 39* (2001), 16, pp. 1881-1897
[14] Sun, X., *et al.*, Heat Transfer Augmentation, Endothermic Pyrolysis and Surface Coking of Hydrocarbon Fuel in Manifold Microchannels at a Supercritical Pressure, *International Communications in Heat and Mass Transfer, 161* (2025), 108564
[15] Zhang, J., *et al.,* Cooperative AC/DC Voltage Margin Control for Mitigating Voltage Violation of Rural Distribution Networks With Interconnected DC Link, *IEEE Transactions on Power Delivery, 40* (2025), 2, pp. 1014-1029
[16] Sun, W., *et al.,* Study on Interaction Mechanism between Natural Convection and Forced Convection during Storage and Temperature Rise of Waxy Crude Oil Tank, *Engineering Applications of Computational Fluid Mechanics, 19* (2025), 1, 2498354
[17] Wu, J., *et al.,* Grooved-Porous Composite Wick Structures for Highly Efficient Capillary-Fed Boiling Heat Transfer, *Applied Thermal Engineering, 256* (2024), 124029
[18] Qi, H., *et al.,* Heat Transfer Performance in Energy Piles in Urban Areas: Case Studies for Lambeth College and Shell Centre UK, *Applied Sciences, 10* (2020), 17, 5974
[19] Li, Y., *et al.,* Nucleate Boiling Heat Transfer and Critical Heat Flux in Controllable Droplet Trains Cooling, *Applied Thermal Engineering, 267* (2025), 125824
[20] Abas, *et al.,* Second Order Slip Micropolar MHD Hybrid Nanofluid Flow over a Stretching Surface with Uniform Heat Source and Activation Energy: Numerical Computational Approach, *Results in Engineering, 25* (2025), 104060
[21] Ullah, *et al.,* Thermal Radiation Effects of Ternary Hybrid Nanofluid Flow in the Activation Energy: Numerical Computational Approach, *Results in Engineering, 25* (2025), 104062
[22] Ullah, *et al.,* Modifications of the Optimal Auxiliary Function Method to Fractional Order Fornberg-Whitham Equations, Computer Modeling in Engineering & Sciences, 136 (2023), 022289
[23] Jan, *et al.,* Modification of OHAM for Multi-Dimensional Time Fractional Model of Navier Stokes Equation, *Fractals, 31* (2023), 2, 2340021
[24] Jan, *et al.,* Fractional View Analysis of the Diffusion Equations via a Natural Atangana-Baleanu Operator, *Alexendria Engineering Journal, 83* (2023), Nov., pp. 19-26
[25] Mumtaz, *et al.,* Chemically Reactive MHD Convective Flow and Heat Transfer Performance of Ternary Hybrid Nanofluid past a Curved Stretching Sheet, *Journal of Molecular Liquids, 390* (2023) 123179
[26] Shaheen, *et al.,* Radiation and Gyrotactic Microorganisms in Walter-B Nanofluid Flow over a Stretching Sheet, *Journal of Radiation Research and Applied Sciences, 18* (2025), 101644
[27] Abas, *et al.,* Magnetohydrodynamic Ternary Hybrid Nanofluid Flow over a Stretching Surface Subject to Thermal Convective and Zero Mass Flux Conditions, *Surface Review and Letters, 31* (2024), 2450028
[28] Ullah, *et al.,* Modification of the Optimal Auxiliary Function Method for Solving Fractional Order KdV Equations, *Fractal Fract. 6* (2022), 288

[29] Ullah, *et al.*, Optimized Neural Network Modeling of Ternary Hybrid Nanofluid Dynamics in Double Rotating Disks with Radiation and Cattaneo-Christov Heat Flux, *Journal of Radiation Research and Applied Sciences, 18* (2025), 101449
[30] Mahariq, *et al.*, Levenberg-Marquardt Recurrent Neural Network for Heat Transfer in Ternary Hybrid Nanofluid Flow with Nonlinear Heat Source-Sink, *Advances in Mechanical Engineering, 17* (2025), 6, pp. 1-25.
[31] Ullah, H., *et al*., Levenberg-Marquardt Backpropagation for Numerical Treatment of Micropolar Flow in a Porous Channel with Mass Injection, *Complexity, 2021* (2021), 5337589
[32] Kanan, M., *et al*., Intelligent Computing Paradigm for Second-Grade Fluid in a Rotating Frame in a Fractal Porous Medium, *Fractals, 31* (2023), 8, 2340175
[33] Rashidi, M. M., Abbasbandy, S., Analytic Approximate Solutions for Heat Transfer of a Micropolar Fluid through a Porous Medium with Radiation, *Communications in Noninear Science and Numerical Simulation, 16* (2011), 4, pp. 1874-1889

Paper submitted: December 18, 2024
Paper revised: February 17, 2025
Paper accepted: May 8, 2025